Author(s): D'Angelo, Stefano

Title: New Family of Wave-Digital Triode Models

Year: 2013

Version: Post print / Accepted author version

Please cite the original version:

S. D Angelo, J. Pakarinen, and V. Välimäki. New Family of Wave-Digital Triode Models. IEEE Trans. Audio, Speech, and Lang. Process., vol. 21, no. 2, pp. 313 321, February 2013.

New Family of Wave-Digital Triode Models

Stefano D'Angelo, Jyri Pakarinen and Vesa Välimäki*, *Senior Member, IEEE*

***Abstract*—A new family of wave-digital vacuum tube triode models is presented. These models are inspired by the triode model by Cardarilli *et al.*, which provides realistic simulation of the triode's transconductance behavior, and hence high accuracy in saturation conditions. The triode is modeled as a single memoryless nonlinear three-port wave digital filter element in which the outgoing wave variables are computed by locally applying the monodimensional secant method to one or two port voltages, depending on whether the grid current effect is taken into account. The proposed algorithms were found to produce a richer static harmonic response, introducing comparable or less aliasing and requiring approximately 50% less CPU time than previous models. The proposed models are suitable for real-time virtual analog circuit simulation.**

***Index Terms*—Acoustic signal processing, amplifiers, circuit simulation, music, wave digital filters.**

I. Introduction

DIGITAL simulation of analog circuitry, also called virtual analog modeling, is currently a vibrant area of research [1], [2], [3]. Software and hardware implementations of modern virtual analog models serve as convenient alternatives for expensive, bulky, and fragile analog equipment such as tube guitar amplifiers. Also, the flexibility of DSP techniques allows simulation of a wide variety of analog circuits with little effort [4].

Various techniques have been used to simulate tube amplifiers [5]. The commercial applications may roughly be divided into two categories; those using black-box modeling, and those using white-box modeling. The black-box modeling approaches work by stimulating the real-world equipment with various input signals and confronting them with the corresponding outputs [6], [7], [8], [9], [10].

The other approach, white-box modeling, employs physics-based simulation techniques, and is especially useful when the system schematics are available. One of the challenges in white-box simulation methods is that real audio circuits are usually rather complex, which often results in a high computational load. Different techniques have been applied for the task, e.g., [11], [12], [13], [14], [15], [16].

Manuscript received January 13, 2012; revised June 10, 2012; accepted September 24, 2012.

S. D'Angelo is with the Department of Signal Processing and Acoustics, Aalto University, School of Electrical Engineering, P.O. Box 13000, FI-00076 AALTO, Espoo, Finland (email: stefano.d'angelo@aalto.fi).

S. D'Angelo's research is funded by the CIMO Centre for International Mobility and by the GETA Graduate School in Electronics, Telecommunications and Automation.

J. Pakarinen was with the Department of Signal Processing and Acoustics, Aalto University, School of Electrical Engineering (email: jyri.pakarinen@gmail.com). He currently works for Dolby Sweden AB, Stockholm, Sweden.

V. Välimäki is with the Department of Signal Processing and Acoustics, Aalto University, School of Electrical Engineering (phone: +358 9 470 25749, fax: +358 9 460 224, email: vesa.valimaki@aalto.fi).

This article uses a white-box modeling approach based on Wave Digital Filters (WDFs) [17]. In the literature, WDFs have been extensively used to model triodes [18], [19], [20] and other circuitry usually found in tube amplifiers [21], [22]. Recently, the WDF theory has been extended by introducing new adapters to match polarities and sign conventions among interconnected subcircuits [23]. The reader is encouraged to refer to comprehensive resources on the topic for further info [17], [24], [25], [26].

One of the most critical aspects in developing such a white-box amplifier simulator is the choice of the tube model, i.e., the set of equations that describe the tube's behavior. Several large-signal triode models have been developed so far and especially in recent years, with different approaches: physical [27], [28], circuital [29], [30], phenomenological [31], [32], interpolative [33], and mixed physical-interpolative [34]. A comprehensive introduction to the topic can be found in [35].

Most of the WDF tube amplifier simulators in the literature [18], [19], [20], [15], [21], [22] use Koren's triode model [31], probably for historical rather than technical reasons, since other models [28], [33], [34] were shown to provide more realistic simulation of the triode's behavior. Among these, the model proposed by Cardarilli *et al.* [34] is particularly appealing because of its high accuracy in saturation conditions and because its parameters can be extracted directly from datasheets, requiring no real-world measurements.

This paper introduces a new family of WDF triode models inspired by the Cardarilli triode model [34]. While the original paper contains an implementation for the SPICE circuit simulator, the algorithms hereby proposed are the first to make such and other similar models suitable for real-time sound processing.

Section II discusses some basic results of the WDF theory that are needed for introducing the new models presented in Section III. Section IV describes the common-cathode triode stage circuit as a case study for which two WDF simulators are created using the new WDF triode models and then confronted with two corresponding previous simulators employing Koren's model [18], [19]. Section V compares the results obtained from the four simulators, evaluating the introduced static harmonic distortion using time-frequency analysis techniques, such as logarithmic swept-sine analysis [36], and investigating how much aliasing is produced and what is the performance of the underlying algorithms. Section VI concludes this paper.

II. WDF Basics

WDFs allow represention of electric, mechanic, or acoustic systems as an interconnected network of digital filters [24], [25], [37]. In practice, each individual circuit component is

mapped into a simple digital filter, and the interconnections between these components (series or parallel) map into bidirectional signal routing blocks. The physical parameters of the circuit components (e.g., resistance, capacitance) determine the signal scattering coefficients inside the routing blocks. Run-time control of any of the circuit element values is easily implemented by varying these scattering coefficients, provided that the control rate is slower than the audio rate, as is typical in analog audio circuits. One of the most intriguing aspects of WDFs is that despite their modular structure, impedance loading effects are inherently simulated in a realistic manner.

This section presents a subset of results of the WDF theory that are strictly needed to introduce the new family of WDF triode models.

A. WDF Wave Decomposition

The WDF formalism [17] deals with bidirectional wave variables (signals entering and leaving WDF components) rather than Kirchhoff variables (voltage and current). Technically, the wave variables a and b may be obtained from the Kirchhoff variables V (voltage) and I (current) using a computational variable called port resistance R_0:

$$\begin{bmatrix} a \\ b \end{bmatrix} = \begin{bmatrix} 1 & R_0 \\ 1 & -R_0 \end{bmatrix} \begin{bmatrix} V \\ I \end{bmatrix}. \tag{1}$$

It should be noted that R_0 is purely a computational tool for resolving the implicit relation between V and I in WDF networks, and it should not be confused with the physical resistance value of an electric component. The wave-to-Kirchhoff variable conversion is easily deduced from Eq. (1) as

$$V = \frac{a+b}{2}, \qquad I = \frac{a-b}{2R_0}.$$

Using (1) together with the bilinear mapping between analog and digital domains (see, e.g., [25]), the basic electric circuit components are transformed into digital filters. These WDF circuit elements are connected to each other using signal routing blocks, called adaptors. Three-port adaptors are typically used, so that the entire modeling structure results as a binary tree [37]. Thus, the adaptors are the nodes of the tree, while circuit components are the leaves. One of the leaves is selected as the root of the tree, and a simulation cycle consists of evaluating the waves from the leaves to the root, computing the wave scattering at the root, and propagating the waves back to the leaves.

When nonlinearities are to be modeled, it is most convenient to place the nonlinear component at the root of the binary tree to avoid introducing uncomputable delay-free loops [37]. Thus, basic WDF structures inherently support having only a single nonlinear component in the circuit. However, several approaches to wave-digital modeling of circuits with single nonlinearities have been developed, ranging from the simple insertion of the nonlinearity as the root element, e.g., [38], to integrating WDFs with numerical techniques that guarantee better accuracy [39] and even to automatic methods for construction of wave-digital structures [40], to name a few. None of these techniques, however, allow delay-free connection of multiple nonlinear WDF elements.

B. Multiport Nonlinear WDF Elements

Various electric audio circuits, such as tube amplifiers, consist of several nonlinear circuit components. Obviously, this imposes a problem for WDF modeling, since only one nonlinear component is inherently supported per circuit. This limitation may be resolved by iterating the sub-tree connecting the nonlinear elements at each time step, as suggested in [21], but this is a computationally expensive operation. Therefore, previous WDF modeling approaches have typically inserted a fictitious unit delay into the system [19], [21], [22] when modeling multiple nonlinearities, but this is a less elegant approach and it causes stability problems in certain conditions.

In this paper we use another approach, suggested in [26], [41], which consists in combining all nonlinear elements and their interconnections as a single multiport nonlinearity, as illustrated for a triode stage in Fig. 1. However, this approach loses the modular structure of the circuit. An additional

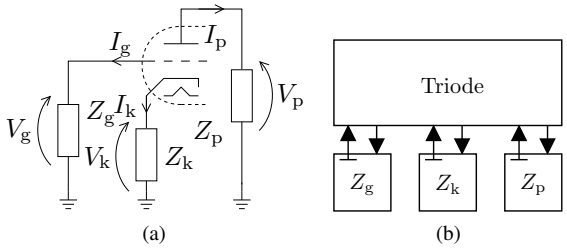

Fig. 1: (a) a typical triode amplifier stage, and (b) its multiport nonlinearity representation.

challenge in WDF modeling is that not all circuit topologies can be mapped into series and parallel connections. Typical problematic topologies in audio circuits include bridge connections and feedback loops, such as the stray capacitances between the terminals of a triode tube.

III. A New Family of WDF Triode Models

Previous WDF triode models typically solved the computability problem due to the dependency of the cathode current on both the grid and the plate voltages by using a fictitious unit delay, as outlined in Section II-B. While such an approximation can be well-founded in simple cases (e.g., [18]), in general it is not and causes accuracy-related problems especially when taking into account the grid current effect. We have therefore decided to develop the new WDF triode models as multiport nonlinear elements.

This section presents the Cardarilli triode model [34], which the new WDF triodes models are inspired by, and then shows the derivation of their WDF implementation. A final consideration on the restrictions imposed on the tube parameters indicates that a whole family of new WDF triode models is obtained.

A. Cardarilli's Triode Model

Cardarilli's triode model [34] uses a mixed physical-interpolative approach by which the constant parameters in the classical formulations for the *space current* I_k and the

grid current $-I_{\mathrm{g}}$ are replaced with splines depending on V_{gk}. The model, according to the current and voltage directions depicted in Fig. 1(a), is then defined as:

$$I_{\mathrm{k}} = G\sqrt{\left(V_{\mathrm{gk}} + \frac{V_{\mathrm{pk}}}{\mu} + h\right)^3}, \tag{2}$$

$$I_{\mathrm{p}} = -I_{\mathrm{k}} - I_{\mathrm{g}}, \tag{3}$$

$$I_{\mathrm{g}} = \begin{cases} \frac{-I_{\mathrm{k}}}{1+D\left(\frac{V_{\mathrm{pk}}}{V_{\mathrm{gk}}-V_{\mathrm{off}}}\right)^K} & \text{when } V_{\mathrm{gk}} > V_{\mathrm{off}} \\ 0 & \text{when } V_{\mathrm{gk}} \leq V_{\mathrm{off}} \end{cases}, \tag{4}$$

where

$$G = \sum_{i=0}^{3} G_i {V_{\mathrm{gk}}}^i, \quad \mu = \sum_{i=0}^{3} \mu_i {V_{\mathrm{gk}}}^i, \quad h = \sum_{i=0}^{3} h_i {V_{\mathrm{gk}}}^i, \tag{5}$$

$$V_{\mathrm{gk}} = V_{\mathrm{g}} - V_{\mathrm{k}}, \quad V_{\mathrm{pk}} = V_{\mathrm{p}} - V_{\mathrm{k}}.$$

In particular, (2) is the classical space-current formulation where G is the tube perveance, μ represents the amplification factor, and h takes into account the effect of the initial electrons velocity. The expression determining the grid current when $V_{\mathrm{gk}} > V_{\mathrm{off}}$ is analogous to the empirical relation proposed in [42] where D and K are measured numerical constants, and to which V_{off} is added to accommodate the contact potential effect.

The original paper [34] also describes a method to calculate the values of G_i, μ_i, h_i, D, K, and V_{off} based on curve fitting of data that is usually found on datasheets. It does also show that this model faithfully reproduces the triode's transconductance behavior, thus providing highly accurate results in saturation conditions unlike other triode models.

B. WDF Implementation

In this subsection we derive a class of WDF models which are based on the Cardarilli triode model.

We denote the incoming wave from each Z_x as a_x and the outgoing wave to each Z_x as b_x and we indicate the port resistance value propagating from each Z_x as R_{0x}. Since in our WDF topology the incoming waves seen by the triode element are the outgoing waves from the subcircuits connected to it and viceversa, we need to "exchange the roles" of a and b in (1) when expressing K variables concerning each Z_x from the "point of view" of the triode element. In particular, the current I_x across each Z_x can be expressed as

$$I_x = \frac{V_x - a_x}{R_{0x}}. \tag{6}$$

Substituting this expression into (2) and (3) and solving for V_{p} yields

$$\begin{aligned} V_{\mathrm{p}} &= V_{\mathrm{k}} + \mu\left(V_{\mathrm{k}} - V_{\mathrm{g}} - h + \alpha\right), \\ V_{\mathrm{p}} &= a_{\mathrm{p}} - R_{0\mathrm{p}}\left(\frac{V_{\mathrm{g}} - a_{\mathrm{g}}}{R_{0\mathrm{g}}} + \frac{V_{\mathrm{k}} - a_{\mathrm{k}}}{R_{0\mathrm{k}}}\right), \end{aligned} \tag{7}$$

where

$$\alpha = \sqrt[3]{\left(\frac{V_{\mathrm{k}} - a_{\mathrm{k}}}{R_{0\mathrm{k}} G}\right)^2}.$$

Confronting these two equations and solving for V_{k} we obtain

$$\begin{aligned} V_{\mathrm{k}} =& \frac{R_{0\mathrm{k}}\left[a_{\mathrm{p}} + \mu\left(V_{\mathrm{g}} + h - \alpha\right)\right] + R_{0\mathrm{p}} a_{\mathrm{k}}}{R_{0\mathrm{p}} + \left(\mu + 1\right) R_{0\mathrm{k}}} \\ &- \frac{R_{0\mathrm{k}} R_{0\mathrm{p}}\left(V_{\mathrm{g}} - a_{\mathrm{g}}\right)}{R_{0\mathrm{g}}\left[R_{0\mathrm{p}} + \left(\mu + 1\right) R_{0\mathrm{k}}\right]}. \end{aligned} \tag{8}$$

From (4), when $V_{\mathrm{gk}} \leq V_{\mathrm{off}}$ we have

$$V_{\mathrm{g}} = a_{\mathrm{g}}, \tag{9}$$

thus (8) becomes

$$V_{\mathrm{k}} = \frac{R_{0\mathrm{k}}\left[a_{\mathrm{p}} + \mu\left(a_{\mathrm{g}} + h - \alpha\right)\right] + R_{0\mathrm{p}} a_{\mathrm{k}}}{R_{0\mathrm{p}} + \left(\mu + 1\right) R_{0\mathrm{k}}}. \tag{10}$$

Otherwise, by substituing (6) into (4) we obtain

$$V_{\mathrm{p}} = V_{\mathrm{k}} + \left(V_{\mathrm{g}} - V_{\mathrm{k}} - V_{\mathrm{off}}\right)\beta, \tag{11}$$

where

$$\beta = \sqrt[K]{-\frac{1}{D}\left(\frac{R_{0\mathrm{g}}}{R_{0\mathrm{k}}}\frac{a_{\mathrm{k}} - V_{\mathrm{k}}}{a_{\mathrm{g}} - V_{\mathrm{g}}} + 1\right)}.$$

Confronting (11) with (7) and solving for V_{g} leads to

$$\begin{aligned} V_{\mathrm{g}} =& \frac{R_{0\mathrm{g}}\left[\left(V_{\mathrm{off}} + V_{\mathrm{k}}\right)\beta - V_{\mathrm{k}} + a_{\mathrm{p}}\right] + R_{0\mathrm{p}} a_{\mathrm{g}}}{R_{0\mathrm{g}}\beta + R_{0\mathrm{p}}} \\ &+ \frac{R_{0\mathrm{g}} R_{0\mathrm{p}}\left(a_{\mathrm{k}} - V_{\mathrm{k}}\right)}{R_{0\mathrm{k}}\left(R_{0\mathrm{g}}\beta + R_{0\mathrm{p}}\right)}. \end{aligned} \tag{12}$$

In summary, if $V_{\mathrm{gk}} \leq V_{\mathrm{off}}$ then V_{g} and V_{k} can be expressed as (9) and (10), otherwise as (12) and (8). In both cases, once they are known, V_{p} is determined by (7). Once the voltages are known, the outgoing wave variables can be then computed from (1) as

$$b_x = 2V_x - a_x.$$

Furthermore, (2) and (4) imply that $-I_{\mathrm{k}} \leq I_{\mathrm{g}} \leq 0$, which in turn implies that

$$V_{\mathrm{k}} \geq a_{\mathrm{k}}, \quad V_{\mathrm{g}} \leq a_{\mathrm{g}}, \quad R_{0\mathrm{g}}(a_{\mathrm{k}} - V_{\mathrm{k}}) \leq R_{0\mathrm{k}}(V_{\mathrm{g}} - a_{\mathrm{g}}). \tag{13}$$

Considering the dependency of G, μ and h on V_{g} and V_{k} expressed in (5), when $V_{\mathrm{gk}} \leq V_{\mathrm{off}}$ the only implicit equation is (10). We have implemented a first algorithm that assumes this is always the case, thus not contemplating the grid current effect. This algorithm solves such equation using the secant method root-finding algorithm, whose update formula is in our case

$$V_{\mathrm{k},n} = V_{\mathrm{k},n-1} - f(V_{\mathrm{k},n-1})\frac{V_{\mathrm{k},n-1} - V_{\mathrm{k},n-2}}{f(V_{\mathrm{k},n-1}) - f(V_{\mathrm{k},n-2})},$$

where

$$f(V_{\mathrm{k},n}) = \frac{R_{0\mathrm{k}}\left[a_{\mathrm{p}} + \mu_n\left(a_{\mathrm{g}} + h_n - \alpha_n\right)\right] + R_{0\mathrm{p}} a_{\mathrm{k}}}{R_{0\mathrm{p}} + \left(\mu_n + 1\right) R_{0\mathrm{k}}} - V_{\mathrm{k},n}.$$

The secant method needs two initial values, hence we used $V_{\mathrm{k},0} = a_{\mathrm{k}}$ as a first guess and $V_{\mathrm{k},1} = a_{\mathrm{k}} + f(a_{\mathrm{k}})$ as the second guess, since $f(a_{\mathrm{k}}) \geq 0$ which guarantees that $V_{\mathrm{k},1} \geq a_{\mathrm{k}}$, in accordance with (13).

When also considering the case in which $V_{\mathrm{gk}} > V_{\mathrm{off}}$ we get two implicit equations, hence it would be natural to use a multidimensional root-finding algorithm. For the second algorithm we have avoided that by considering that in most

cases $-I_\mathrm{k} \ll I_\mathrm{g}$, hence it follows that, given (8), the previous algorithm can be used to give a good first approximation for the value of V_k which can be then adjusted by taking into account the grid current effect, if present.

In practice this is done by starting with an initial guess $V_{\mathrm{g},0} = a_\mathrm{g}$ and by first applying the secant method to (8). At this point, if $V_\mathrm{gk} \leq V_\mathrm{off}$ the computation is finished, otherwise the secant method is applied to (12) with $V_{\mathrm{g},1} = a_\mathrm{g} + f(a_\mathrm{g})$, following a similar reasoning as before. When this iteration finishes, V_k is updated and if $|f(V_\mathrm{k})|$ is smaller than a threshold then the computation is finished, otherwise V_k is evaluated again starting from the last values of V_k and V_g, and the algorithm proceeds in a ping-pong fashion.

In both algorithms, (13) is enforced at every step, either by forcing values of V_k and V_g to stay in the specified ranges (initial guesses) or by breaking the current iterative loop without updating values.

Note that while the Cardarilli triode model specifies that $G(V_\mathrm{gk})$, $\mu(V_\mathrm{gk})$, and $h(V_\mathrm{gk})$ are splines and that D, K, and V_off are constant values, our WDF implementation does not impose restrictions on how these values are computed as long as they do not depend on V_p and $G > 0$ and $\mu > 0$. This means that a wide class of parameter interpolation techniques can be used in conjunction with the described algorithms.

IV. Case Study: Common-Cathode Triode Stage

The ubiquitous common-cathode triode gain stage circuit, illustrated in Fig. 2, is a typical building block used in tube amplifiers, and therefore a natural choice for a modeling target. As seen in Fig. 2, the triode has three terminals: plate (p), grid (g), and cathode (k), and each terminal connects to an RC circuit. The currents flowing through the three terminals have been denoted I_p, I_g, and I_k, respectively. The input signal for the triode stage is represented as the voltage V_i, and the capacitor C_i decouples the dc component from the input. The input capacitor C_i is discharged via resistor R_i in case it becomes charged due to grid current I_g.

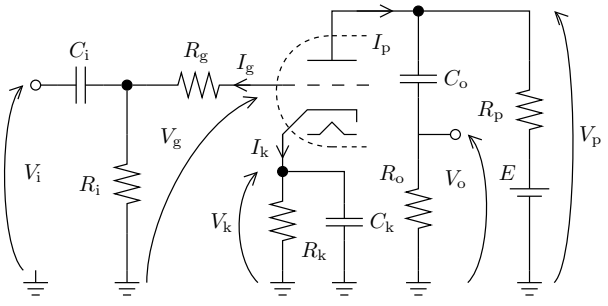

Fig. 2: The common-cathode triode gain stage, typically found in tube amplifiers.

A parallel connection of R_k and C_k forms the cathode circuit, which sets the signal-dependent biasing for the triode. The right-hand branch of the plate circuit consists of an operating voltage source E, and a plate resistor R_p, providing the plate current I_p. The left-hand branch of the plate circuit is formed by a dc decoupling capacitor C_o and load resistance R_o. The amplified output V_o of the triode stage is measured as the voltage over R_o.

Since the amplification provided by the triode tube is nonlinear, the gain stage in Fig. 2 causes rather complex signal-dependent distortion. The dynamic nature of the distortion is partly due to the signal-dependent biasing resulting from the reactive cathode circuit, and partly due to the charging of the input capacitor by grid current with large input signals. However, it should be noted that the linear coloration of the triode gain stage is minimal, apart from the dc attenuation caused by capacitors C_i and C_o.

A. Previous WDF Simulators

The first reported attempt to simulate the common-cathode triode stage using WDFs was presented in [18]. In this approach, the triode was modeled as a nonlinear resistor at the root of the WDF tree. The grid circuit was omitted, and the grid voltage was directly fed as the input signal for the stage. The implicit relation between the grid-to-cathode voltage and cathode current was resolved by delaying the cathode voltage one time sample before evaluating the grid-to-cathode voltage. In effect, the triode stage model in [18] was able to realistically simulate the signal-dependent nonlinearity of the triode tube with reactive cathode circuit, but failed to mimic the dynamic nonlinearities caused by the grid circuit. Also, other dynamic effects due to the impedance loading between triode stages and reactive loads was beyond the capabilites of the model in [18].

An improved WDF triode stage model was presented in [19]. This approach added the grid circuit to the model in [18] via a diode nonlinearity, and thus enabled also simulation of the dynamic nonlinearities caused by grid current, as well as the modeling of impedance loading effects. In practice, the diode – a second nonlinearity in the WDF tree – was connected via a unit delay in order to avoid the implicit relation between the two nonlinearities.

Furthermore, the WDF structures of both simulators suffered from polarity-related issues that were not yet understood by the time the models were proposed. These issues were first described in [23], which also contains an enhanced version of the first simulator. Fig. 3 shows versions of both simulators where WDF polarity inverters are inserted where needed to match polarities among interconnected subcircuits.

B. New WDF Simulators

Two analogous simulators were developed using the new WDF triode models, of which one that takes into account the grid current effect and another that does not. Both share the same WDF structure shown in Fig. 4. Thus, the only difference between them resides in which of the two algorithms described in Section III-B is used.

V. Evaluation

This section confronts the two simulators described in Section IV-A and shown in Fig. 3 with the two analogous simulators described in Section IV-B and shown in Fig. 4. In

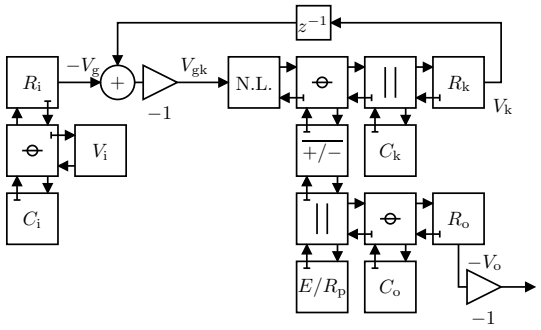

(a) Previous simulator w/o grid current

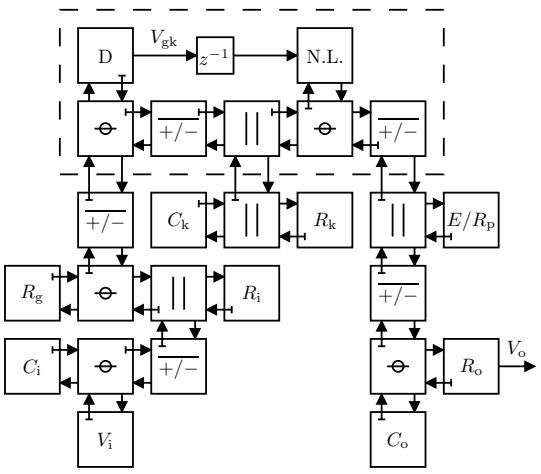

(b) Previous simulator w/ grid current

Fig. 3: Implementations of previous WDF simulators with the addition of WDF polarity inverters. The element N.L. is the nonlinearity.

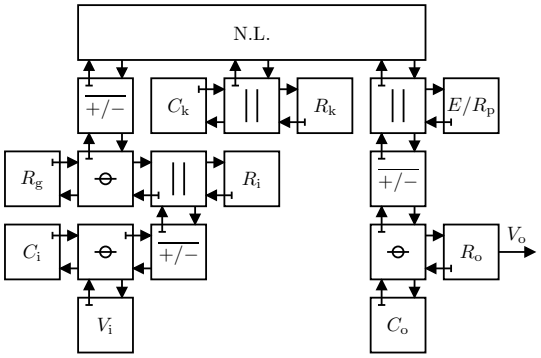

Fig. 4: Implementation of new WDF simulators. The same structure is used in both cases (w/o and w/ grid current).

particular, the triode parameters for the new simulators are computed according to the original triode model paper [34], with the only difference that the values of $G(V_\mathrm{gk})$ and $\mu(V_\mathrm{gk})$ are forced to the minimum positive values G_min and μ_min, respectively, in the rare cases in which they would evaluate to smaller or even negative values. Tables I, II, and III list the parameter values used for the simulations discussed hereafter.

Component	Value
E	250 V
R_i	1 MΩ
R_g	20 kΩ
R_p	100 kΩ
R_o	1 MΩ
C_i	100 nF
C_k	10 μF
C_o	10 nF

TABLE I: Linear components values used for the evaluation of the WDF simulators.

Parameter	Value
μ	100
X	1.4
k_G1	1060
k_P	600
k_VB	300 V^2
$R_\mathrm{D+}$	2.7 kΩ
$R_\mathrm{D-}$	100 GΩ

TABLE II: Parameter values for Koren's model (12AX7) used for the evaluation of the WDF simulators.

A. Time-Frequency Output Analysis

We have performed *logsweep analysis* [36] in order to evaluate the static harmonic distortion introduced by each simulator. This technique consists in feeding a system with a fixed amplitude logarithmically swept sine and then convolving the system response with the time-reversed and amplitude weighted excitation signal. The result of this operation is an impulse response signal where the linear response and individual harmonic distortion components are separated from each other in time. The input signal we used is a 2 seconds long, 4 V logarithmically swept sine from 20 Hz to 100 kHz at a 384-kHz sample rate. Fig. 5 shows the normalized spectrograms of the obtained output signals and Fig. 6 depicts the normalized harmonic spectra up to the 10^th harmonic of such signals.

Both figures clearly show that the new simulators produce an overall richer harmonic response, especially when it comes

Param.	Value	Param.	Value
G_0	1.102 mA / V$^{2/3}$	μ_0	99.705
G_1	15.12 μA / V$^{5/3}$	μ_1	-22.98 / kV
G_2	-31.56 μA / V$^{8/3}$	μ_2	-0.4489 / V^2
G_3	-3.286 μA / V$^{11/3}$	μ_3	-22.27 / kV^3
G_min	1 nA / V$^{2/3}$	μ_min	10^{-9}
h_0	0.6 V	V_off	-0.2 V
h_1	0	D	0.12
h_2	0 / V	K	1.1
h_3	0 / V^2		

TABLE III: Parameter values for the Cardarilli model (12AX7) used for the evaluation of the WDF simulators.

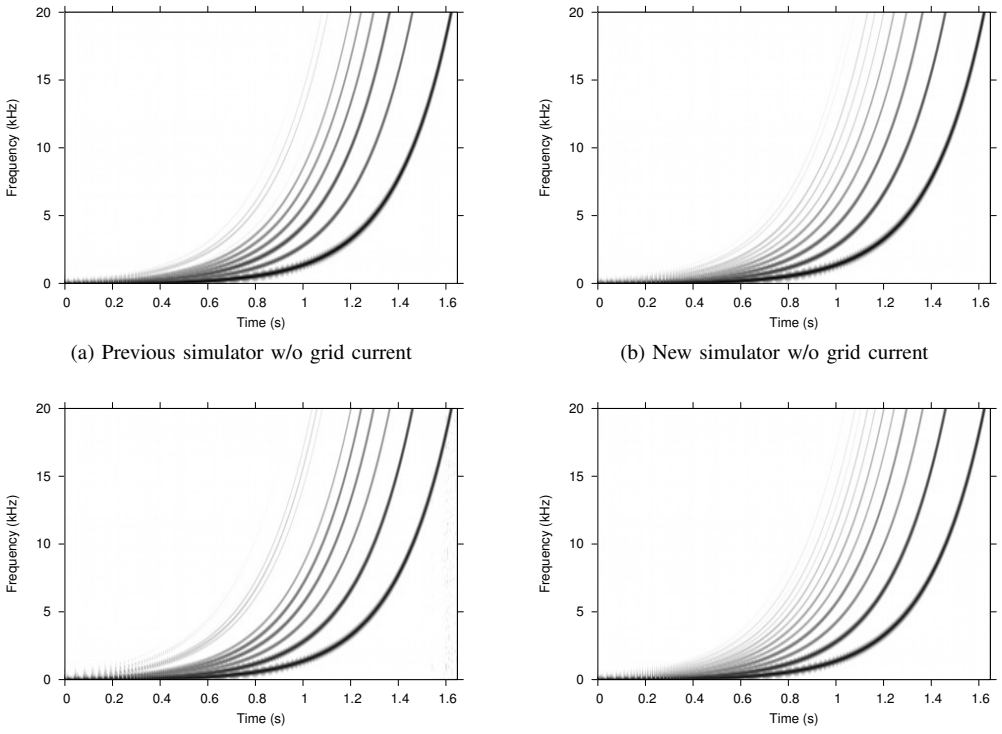

(a) Previous simulator w/o grid current

(b) New simulator w/o grid current

(c) Previous simulator w/ grid current

(d) New simulator w/ grid current

Fig. 5: Normalized spectrograms of the outputs obtained by exciting the WDF simulators operating at 384 kHz sample rate with a 2 seconds long, 4 V logarithmically swept sine from 20 Hz to 100 kHz. The color scale ranges from -60 dB (white) to 0 dB (black).

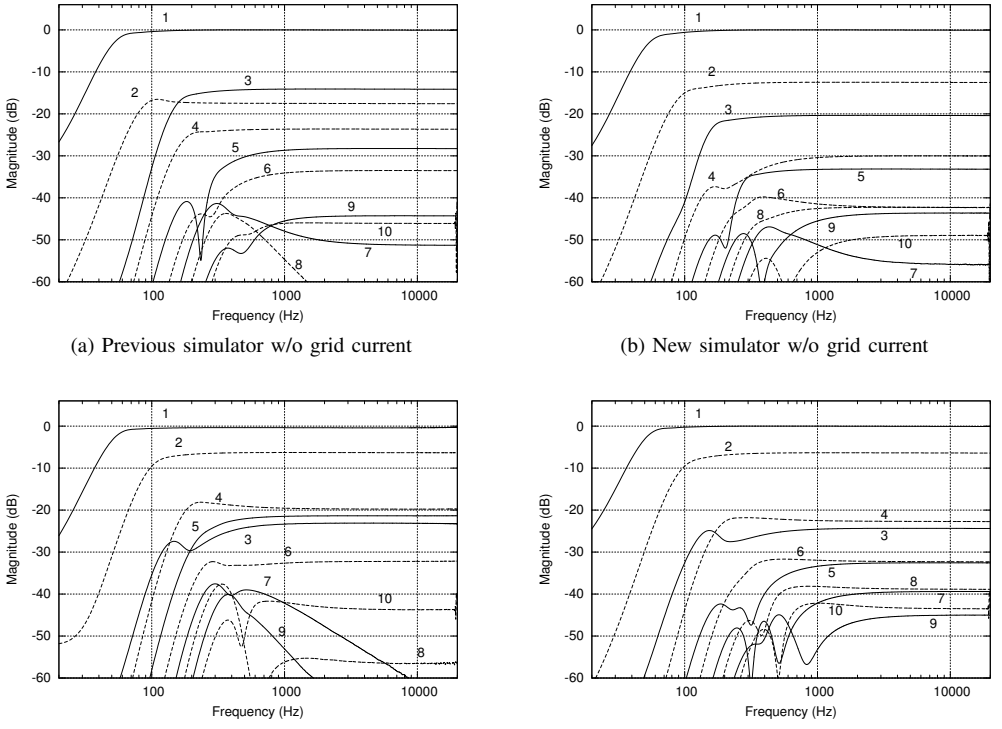

(a) Previous simulator w/o grid current

(b) New simulator w/o grid current

(c) Previous simulator w/ grid current

(d) New simulator w/ grid current

Fig. 6: Normalized harmonic spectra up to the 10^{th} harmonic of the outputs obtained by exciting the WDF simulators operating at a 384-kHz sample rate with a 2 seconds long, 4 V logarithmically swept sine from 20 Hz to 100 kHz and applying the analysis technique described in [36] on the output signals. The fundamental and odd harmonic responses are represented by solid lines, even harmonic responses by dashed lines.

to higher order harmonics. In particular, the outputs obtained from the previous simulators show a substantial lack of the 7^{th} and 8^{th} harmonics, which also exhibit a frequency-dependent behavior at high frequencies, unlike other harmonics. The same is also true for the 9^{th} harmonic in the output obtained from the previous simulator with grid current effect and partially true for the 7^{th} harmonic in the output from the new simulator without the grid current effect.

Fig. 6 also shows how the harmonic response of the two simulators contemplating the grid current effect is substantially equivalent up to the 4^{th} harmonic, unlike what happens with the other two simulators. The former also produce stronger even harmonics when compared to the latter, which is consistent with the concept that the grid current actively contributes to the asymmetricity in tube clipping.

Also worth noticing is that the magnitudes of the harmonics produced by the new simulator with grid current effect are decreasingly sorted within their parity group at high frequencies. In other words, the magnitude of the 2^{nd} harmonic is greater than that of the 4^{th} harmonic, which is in turn larger than that of the 6^{th} harmonic, etc. and the same holds true for odd harmonics.

B. Output Aliasing Analysis

In order to obtain some indication on the amounts of aliasing introduced by the simulators, we have stimulated them with a 1 second long, 4 V, 1.5708 kHz sine wave at a 96-kHz sample rate, then applied a Dolph-Chebyshev window with -100 dB side-lobe level to the outputs, normalized them so that the fundamental is at the 0 dB level, computed the spectra of such signals and filtered out the harmonic components. Fig. 7 shows the results of this analysis.

The two new simulators produce slightly more aliasing than the previous one without grid current effect, but significantly less aliasing than the one with grid current. The relatively high level of aliasing in the output produced by this last simulator is due both to the presence of a discontinuity in the derivative of the transfer characteristic of the diode nonlinearity, since it is modeled as a piecewise linear resistor, and to the extra delay unit between the diode element and the plate-to-cathode nonlinear resistor element.

C. Algorithm Performance

The four simulators have been tested with various input signals, including both synthesized and recorded sounds, at different input gain levels and at different sample rates in order to obtain a rough estimation of the relative speed performance of their algorithms. The tests revealed that the new algorithms, despite the increased implementation complexity for each iteration and despite not using previous outputs as initial guesses, are approximately two times faster in average than the algorithms based on Koren's model. This necessarily means that it takes less iterations, in average, for the new algorithms to converge.

We have, indeed, found out that in rare but actually occuring cases, previous algorithms require an overwhelmingly high number of iterations to converge, and especially when the input signal has a high gain. Furthermore, the use of previous outputs as initial guesses on one side decreases the average number of iterations, but on the other makes this phenomenon more evident when the input signal has significant frequency components approaching the Nyquist limit.

The tested implementations are relatively unoptimized and designed to be as similar to each other as possible. They were executed on an Acer Extensa 5220 laptop with 1 GB RAM running ArchLinux x86-64. The results in terms of CPU usage are reported in Table IV.

SR	Prev	Prev w/ gc	New	New w/ gc
96 kHz	29.87%	31.99%	**11.02%**	14.80%
192 kHz	45.69%	53.11%	**20.89%**	29.29%
384 kHz	94.21%	107.71%	**42.80%**	49.72%

TABLE IV: Average CPU usage detected by processing a set of input signals at different sample rates, after previous oversampling, and at different input gain levels.

VI. Conclusion

A new family of WDF triode models was presented. These new models are inspired by the triode model by Cardarilli *et al.* [34], and they perform more realistically than the previous WDF models [18], [19] based on Koren's model [31], especially in the strongly saturating case. The new models do not require the use of extra delay units in feedback loops and are memoryless. Two models of this new family were compared to the corresponding previous models [18], [19] and they were found to produce a richer static harmonic response, introducing comparable or less aliasing and requiring about 50% less CPU time.

The iterative algorithm on which these new WDF triode models are based has little dependency on how the parametrization is actually done, hence it is possible to try different such solutions more easily than before. The new models do not take into account stray capacitance effects between the tube electrodes, hence further investigation is also needed in this area.

Supplementary material to this paper, including sound examples, can be accessed at http://www.acoustics.hut.fi/go/ieee-taslp-2012-tube/.

Acknowledgment

We acknowledge fruitful discussions with Julian Parker.

References

[1] V. Välimäki, F. Fontana, J. O. Smith, and U. Zölzer, "Introduction to the special issue on virtual analog audio effects and musical instruments," *IEEE Trans. Audio, Speech and Lang. Process.*, vol. 18, no. 4, pp. 713–714, May 2010.

[2] J. Pakarinen, V. Välimäki, F. Fontana, V. Lazzarini, and J. S. Abel, "Recent advances in real-time musical effects, synthesis, and virtual analog models," *EURASIP J. Advances Signal Process.*, pp. 1–15, 2011.

[3] D. T. Yeh, "Automated physical modeling of nonlinear audio circuits for real-time audio effects–part II: BJT and vacuum tube examples," *IEEE Trans. Audio, Speech and Lang. Process.*, vol. 20, no. 4, pp. 1207–1216, May 2012.

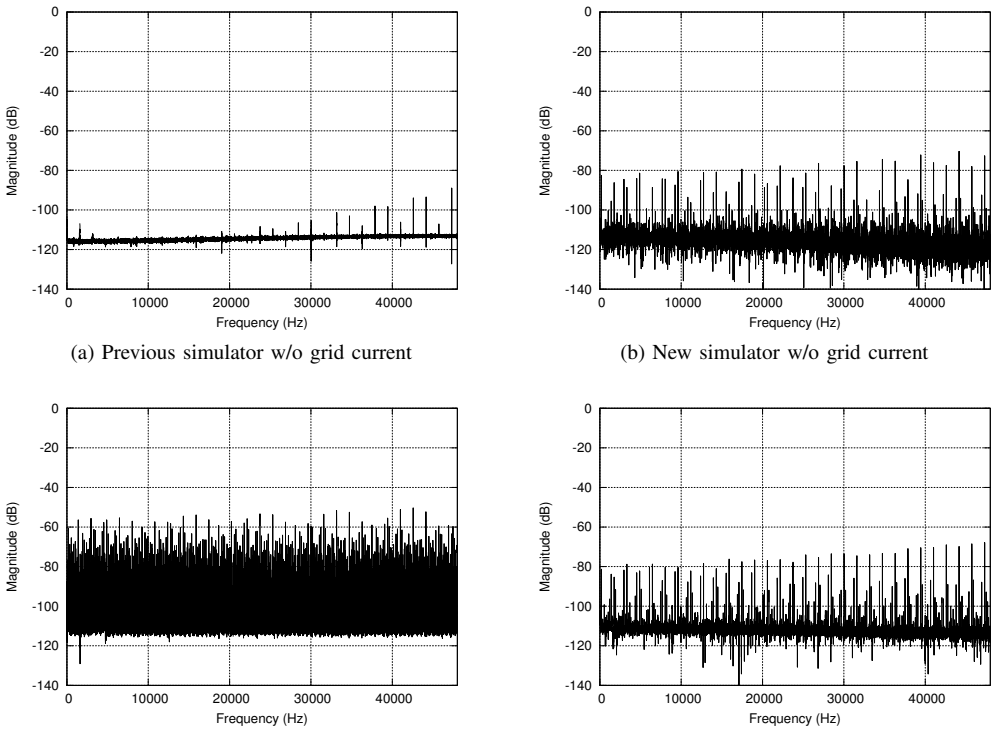

(a) Previous simulator w/o grid current

(b) New simulator w/o grid current

(c) Previous simulator w/ grid current

(d) New simulator w/ grid current

Fig. 7: Spectra of the residual signals obtained by filtering out the harmonic components from the normalized outputs obtained by exciting the WDF simulators operating at a 96-kHz sample rate with a 1 second long, 4 V, 1.5708 kHz sine wave. The output signals were first applied a Dolph-Chebyshev window with -100 dB side-lobe level and then normalized so that the magnitude of the fundamental was at the 0 dB level.

[4] V. Välimäki, S. Bilbao, J. O. Smith, J. S. Abel, J. Pakarinen, and D. Berners, *DAFX – Digital Audio Effects*, 2nd ed. Chichester, UK: Wiley, 2011, ch. Virtual Analog Effects, pp. 473–522.

[5] J. Pakarinen and D. T. Yeh, "A review of digital techniques for modeling vacuum-tube guitar amplifiers," *Comput. Music J.*, vol. 33, no. 2, pp. 85–100, June 2009.

[6] A. Novak, L. Simon, and P. Lotton, "Analysis, synthesis, and classification of nonlinear systems using synchronized swept-sine method for audio effects," *EURASIP J. Advances Signal Process.*, pp. 1–8, 2010.

[7] B. Bank, "Computationally efficient nonlinear Chebyshev models using common-pole parallel filters with the application to loudspeaker modeling," in *Proc. 130th AES Convention*, London, UK, May 2011.

[8] J. Kemp and H. Primack, "Impulse response measurement of nonlinear systems: Properties of existing techniques and wide noise sequences," *J. Audio Eng. Soc.*, vol. 59, no. 12, pp. 953–963, December 2011.

[9] R. Cauduro Dias de Paiva, J. Pakarinen, and V. Välimäki, "Reduced-complexity modeling of high-order nonlinear audio systems using swept-sine and principal component analysis," in *Proc. 45th AES Conf.*, Helsinki, Finland, March 2012.

[10] F. G. Germain, J. S. Abel, P. Depalle, and M. M. Wanderley, "Uniform noise sequences for nonlinear system identification," in *Proc. 15th Intl. Conf. Digital Audio Effects (DAFx-12)*, York, UK, September 2012, pp. 241–244.

[11] D. T. Yeh and J. O. Smith, "Discretization of the '59 Fender Bassman tone stack," in *Proc. 9th Intl. Conf. Digital Audio Effects (DAFx-06)*, Montreal, Canada, September 2006, pp. 1–6.

[12] ——, "Simulating guitar distortion circuits using wave digital and nonlinear state-space formulations," in *Proc. 11th Intl. Conf. Digital Audio Effects (DAFx-08)*, Espoo, Finland, September 2008, pp. 19–26.

[13] D. T. Yeh, J. S. Abel, and J. O. Smith, "Automated physical modeling of nonlinear audio circuits for real-time audio effects–part I: Theoretical development," *IEEE Trans. Audio, Speech and Lang. Process.*, vol. 18, no. 4, pp. 728–737, May 2010.

[14] J. Macak and J. Schimmel, "Real-time guitar tube amplifier simulation using an approximation of differential equations," in *Proc. 13th Intl. Conf. Digital Audio Effects (DAFx-10)*, Graz, Austria, September 2010, pp. 59–62.

[15] ——, "Real-time guitar preamp simulation using modified blockwise method and approximations," *EURASIP J. Advances Signal Process.*, pp. 1–10, 2011.

[16] R. C. D. de Paiva, S. D'Angelo, J. Pakarinen, and V. Välimäki, "Emulation of operational amplifiers and diodes in audio distortion circuits," *IEEE Trans. Circ. and Systems – II: Express Briefs*, vol. 59, no. 10, pp. 688–692, October 2012.

[17] A. Fettweis, "Wave digital filters: theory and practice," *Proc. IEEE*, vol. 74, no. 2, pp. 270–327, February 1986.

[18] M. Karjalainen and J. Pakarinen, "Wave digital simulation of a vacuum-tube amplifier," in *Proc. Intl. Conf. on Acoustics, Speech, and Signal Process. (ICASSP)*, vol. 5, Tolouse, France, May 2006, pp. 153–156.

[19] J. Pakarinen and M. Karjalainen, "Enhanced wave digital triode model for real-time tube amplifier emulation," *IEEE Trans. Audio, Speech and Lang. Process.*, vol. 18, no. 4, pp. 738–746, May 2010.

[20] M. Fink and R. Rabenstein, "A Csound opcode for a triode stage of a vacuum tube amplifier," in *Proc. 14th Intl. Conf. Digital Audio Effects (DAFx-11)*, Paris, France, September 2011, pp. 367–370.

[21] J. Pakarinen, M. Tikander, and M. Karjalainen, "Wave digital modeling of the output chain of a vacuum tube amplifier," in *Proc. 12th Intl. Conf. Digital Audio Effects (DAFx-09)*, vol. 2, Como, Italy, September 2009, pp. 1–4.

[22] R. C. D. de Paiva, J. Pakarinen, V. Välimäki, and M. Tikander, "Real-time audio transformer emulation for virtual tube amplifiers," *EURASIP J. Advances Signal Process.*, pp. 1–15, 2011.

[23] S. D'Angelo and V. Välimäki, "Wave-digital polarity and current inverters and their application to virtual analog audio processing," in *Proc. Intl. Conf. on Acoustics, Speech, and Signal Proc. (ICASSP)*, Kyoto, Japan, March 2012.

[24] J. Smith, "Wave digital filters," in *Physical Audio Signal Processing*. http://ccrma.stanford.edu/~jos/pasp/, accessed 02/10/2011, online book.

[25] V. Välimäki, J. Pakarinen, C. Erkut, and M. Karjalainen, "Discrete-time modelling of musical instruments," *Reports on Progress in Physics*, vol. 69, no. 1, pp. 1–78, January 2006.

[26] G. De Sanctis and A. Sarti, "Virtual analog modeling in the wave-digital domain," *IEEE Trans. Audio, Speech and Lang. Process.*, vol. 18, no. 4, pp. 715–727, May 2010.
[27] F. Broyd, "Modélisation et simulation des circuits à tubes avec isspice3," *Electronique Radio Plans*, no. 553, pp. 69–73, December 1993.
[28] K. Dempwolf and U. Zölzer, "A physically-motivated triode model for circuit simulations," in *Proc. 14th Intl. Conf. Digital Audio Effects (DAFx-11)*, Paris, France, September 2011, pp. 257–264.
[29] W. M. Leach, Jr., "Spice models for vacuum-tube amplifiers," *J. Audio Eng. Soc*, vol. 43, no. 3, pp. 117–126, March 1995.
[30] C. Rydel, "Simulation of electron tubes with SPICE," in *Proc. 98th AES Convention*, Paris, France, February 1995.
[31] N. Koren, "Improved vacuum tube models for SPICE simulations," *Glass Audio*, vol. 8, no. 5, pp. 18–27, 1996.
[32] I. Cohen and T. Hélie, "Measures and parameter estimation of triodes for the real-time simulation of a multi-stage guitar preamplifier," in *Proc. 129th AES Convention*, San Francisco, USA, November 2010.
[33] J. C. Maillet, "A generalized algebraic technique for modeling triodes," *Glass Audio*, vol. 10, no. 2, pp. 2–9, 1998.
[34] G. Cardarilli, M. Re, and L. Di Carlo, "Improved large-signal model for vacuum triodes," in *IEEE Intl. Symp. Circ. and Systems (ISCAS)*, Taipei, Taiwan, May 2009, pp. 3006–3009.
[35] A. Potchinkov, *Simulation von Röhrenverstärken mit SPICE*, 1st ed. Vieweg+Teubner, 2009.
[36] A. Farina, "Simultaneous measurement of impulse response and distortion with a swept-sine technique," in *Proc. 108th AES Convention*, Paris, France, February 2000.
[37] G. De Sanctis, A. Sarti, and S. Tubaro, "Automatic synthesis strategies for object-based dynamical physical models in musical acoustics," in *Proc. 6th Intl. Conf. Digital Audio Effects (DAFx-03)*, London, UK, September 2003, pp. 198–202.
[38] K. Meerkötter and R. Scholtz, "Digital simulation of nonlinear circuits by wave digital filter principles," in *IEEE Intl. Symp. Circ. and Systems (ISCAS)*, Portland, USA, May 1989, pp. 720–723.
[39] D. Fränken and K. Ochs, "Wave digital simulation of nonlinear electrical networks by means of passive Runge-Kutta methods," in *IEEE Intl. Symp. Circ. and Systems (ISCAS)*, Sydney, Australia, May 2001, pp. 469–472.
[40] A. Sarti and G. De Sanctis, "Systematic methods for the implementation of nonlinear wave-digital structures," *IEEE Trans. Circuits and Systems*, vol. 56, no. 2, pp. 460–472, February 2009.
[41] S. Petrausch and R. Rabenstein, "Wave digital filters with multiple nonlinearities," in *Proc. 12th European Signal Process. Conf. (EUSIPCO)*, Vienna, Austria, September 2004, pp. 77–80.
[42] K. Spangenberg, *Vacuum Tubes*. McGraw-Hill Book Co., 1948.

Stefano D'Angelo was born in Vallo della Lucania, Italy, in 1987. He received the M.S. degree in Computer Engineering from Politecnico di Torino in 2010. He is currently a doctoral student at the Department of Signal Processing and Acoustics at the Aalto University School of Electrical Engineering, Espoo, Finland. His main research interests are audio programming languages and digital emulation of electric audio circuits.

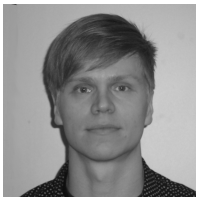

Jyri Pakarinen was born in Lappeenranta, Finland in 1979. He received the M.S. and D.S. (Tech.) degrees in acoustics and audio signal processing from the Helsinki University of Technology in 2004 and 2008, respectively. Dr. Pakarinen worked as a researcher in the Aalto University, Finland, from 2002 until 2011. His main research foucsed on sound synthesis through physical modeling, digital emulation of electric audio circuits, and vibroacoustical measurements. He was the Lead Guest Editor of a special issue of the EURASIP Journal on Advances in Signal Processing in 2011. Dr. Pakarinen is currently working for Dolby Sweden AB in Stockholm, Sweden.

Vesa Välimäki (S90–M92–SM99) received the M.S. (Tech.), the Licentiate of Science in Technology, and the Doctor of Science in Technology degrees, all in electrical engineering, from the Helsinki University of Technology (TKK), Espoo, Finland, in 1992, 1994, and 1995, respectively.

He was a Postdoctoral Research Fellow at the University of Westminster, London, UK, in 1996. In 1997-2001, he was a Senior Assistant (cf. Assistant Professor) at the TKK Laboratory of Acoustics and Audio Signal Processing, Espoo, Finland. From 1998 to 2001, he was on leave as a Postdoctoral Researcher under a grant from the Academy of Finland. In 2001-2002, he was Professor of signal processing at the Pori unit of the Tampere University of Technology, Pori, Finland. He was appointed Docent in signal processing at the Pori unit of the Tampere University of Technology in 2003. In 2006-2007, he was the Head of the TKK Laboratory of Acoustics and Audio Signal Processing. He is currently Professor in the Department of Signal Processing and Acoustics, Aalto University, Espoo, Finland. In 2008-2009, he was on sabbatical as a Visiting Scholar at the Center for Computer Research in Music and Acoustics (CCRMA), Stanford University, Stanford, CA. His research interests include audio effects processing, digital filtering, sound synthesis, and acoustics of musical instruments.

Prof. Välimäki is a senior member of the IEEE, a fellow of the Audio Engineering Society, a member of the Finnish Musicological Society, and a life member of the Acoustical Society of Finland. In 2000-2001, he was Secretary of the IEEE Finland Section. He was President of the Finnish Musicological Society in 2003-2005. In 2008, he was the Chairman of DAFx-08, the 11th International Conference on Digital Audio Effects (Espoo, Finland). He has served as an Associate Editor of the IEEE TRANSACTIONS ON AUDIO, SPEECH AND LANGUAGE PROCESSING and of the IEEE SIGNAL PROCESSING LETTERS. He was the Lead Guest Editor of a special issue of the IEEE SIGNAL PROCESSING MAGAZINE in 2007 and of a special issue of the IEEE TRANSACTIONS ON AUDIO, SPEECH AND LANGUAGE PROCESSING in 2010. He is a member of the Audio and Acoustic Signal Processing Technical Committee of the IEEE Signal Processing Society.